Recent Research Developments in Surface Science, 1 (2004) 75-99

SURFACE SCIENCE MEETS CATALYSIS RESEARCH: IRON OXIDE FILMS FOR *in-situ* MODEL CATALYSIS

Wolfgang Ranke*, Osama Shekhah

Fritz Haber Institute of the Max Planck Society
Faradayweg 4-6, DE-14195 Berlin, Germany
Tel +49 30 8413 4523; Fax +49 30 8413 4401;

*corresponding author, e-mail: ranke@fhi-berlin.mpg.de

Short (running) title: Iron oxide films for model catalysis

Submitted 20 February 2004

ABSTRACT

An in-depth model catalysis study on a complex system is reviewed. Both unpromoted and potassium-promoted iron oxide model catalysts films of single crystalline quality are prepared and characterized in ultrahigh vacuum (UHV) using surface science methods. In order to bridge the pressure and material gap for the catalytic dehydrogenation of ethylbenzene to styrene in presence of steam, this reaction is studied at reactive gas pressures between 10^{-6} and 36 mbar. The samples are transferred under vacuum into an stagnation point micro-flow reactor where the reaction is studied, followed by post-reaction characterization in UHV. Clean hematite Fe_2O_3 is an excellent catalyst but deactivates quickly by reduction and by coking. Addition of H_2O limits reduction to the oxidation state of magnetite Fe_3O_4 and counteracts coking. Both deactivation mechanisms can be avoided by addition of some O_2 to the feed. Potassium has basically the same functions as O_2. It does not seem to be involved in the catalytic dehydrogenation step but rather to block active sites if its concentration is high. Long-term deactivation occurs mainly by potassium removal in form of volatile KOH. Regeneration by "steaming" in pure H_2O accelerates this process while ethylbenzene in the feed stabilizes potassium. This is ascribed to the formation of non-volatile K_2CO_3 which is an intermediate in potassium catalysed coke removal. The addition of O_2 instead of K-promotion may be an alternative reaction route.

Keywords
Auger electron spectroscopy, carbonaceous deposits, catalysis, deactivation, dehydrogenation, ethylbenzene, iron oxide, low energy electron diffraction, potassium, promotor, single crystal, styrene, oxygen

1. INTRODUCTION

Surface science is the regime of low pressures, small single crystalline samples, advanced and complete surface characterization, small amounts of adsorbed species and controlled modification of surface composition and structure (including defects) [1,2]. Catalysis is the regime of high pressures, temperatures and coverages, dispersed, polycrystalline or even porous samples with ill defined surfaces of large area which may undergo fast and dramatic changes during the catalytic reaction [3].

The difficulties in the transferability of surface science results to real catalysis conditions and vice versa have been expressed in terms of a number of 'gaps' between both fields of research:

Pressure p (and temperature T and coverage Θ) gap (p-T-Θ-gap): Can low-pressure (and low-temperature, low-coverage) data on adsorption/desorption be extrapolated to realistic conditions? Are surface and bulk phases the same at low and high p,T, Θ?

Material gap: How relevant are single crystal studies as models for complex real catalysts? Has the "working" catalyst the same structure, composition etc. as before or after reaction at low T and low p? Do defects at the surface or in the bulk form under reaction conditions? Are they relevant for the catalytic mechanism? Occurs dynamic or entropic "stabilisation" of metastable phases or structures (everything moves at high T)?

Reaction gap: Is the considered reaction at model catalysis conditions really catalytic or is it stoichiometric? Does it follow the same path? How important are rare events which are hardly observable at low pressures?

Engineering gap: Is a kinetic modeling of the real catalytic reaction possible using physically and chemically meaningful parameters? Is the transfer of ideas from the surface science approach into process technology possible? Can safety considerations be met?

Theory gap: Theory can still only treat comparatively simple systems (max ~1000 atoms), at zero-*T*. Dynamically or entropically stabilized structures are still not feasible. The reliability of methods is still under discussion.

The idea is not new to overcome the *p*-*T*-Q-gap by combination of a conventional UHV chamber with a high-pressure cell [4] and different types of arrangements have been proposed (some of them are discussed in [5]). Preparation and characterization of a catalytically interesting surface is performed in UHV using the methods of surface science and after that the sample is transfered under vacuum into a high-pressure cell where catalytic conversion measurements can be performed at pressures far enough away from UHV to yield information relevant to real catalysis conditions.

The material gap problem is more difficult to overcome. In the past, catalytically relevant surface science studies have concentrated on apparently simple catalytic substrates (mostly metals like Pt, Pd…) and simple reactants (like CO, O_2, H_2O, NO_x, N_2, H_2 NH_3…) where changes of the catalyst phase and composition under the atmosphere of the high-pressure reaction were not expected. But even metallic systems are often not 'simple'. In-situ measurements on Cu[6] and Ag[7] catalysts showed that activity may only be generated under the influence of the reactants at high pressure. And most of the relevant catalysts are even more complex: Oxides, often promoted with alkalis or mixed with other oxides as "structural promotors", metals supported on oxides, doped and impregnated oxides, zeolites, not to speak about encymes in the regime of biochemistry [3]. And most of the relevant reactants are complex. It is likely that catalyst composition, crystallographic phase, defect structure, promotor distribution, size, shape and distribution of supported metal particles under reaction conditions differ considerably from the state before start of the reaction or after queching from reaction conditions. Quenching is a problem in itself. Composition, structure and morphology of the quenched catalyst may depend on the atmosphere during quenching and the velocity of p and T change. The application of in-situ analysis methods is unavoidable in order to shine light on such processes. A number of such in-situ methods has been developed during the last decade which are capable to determine surface and bulk properties during reaction at relevant pressures and temperatures of the relevant reaction gases[8,9]. An important result is that the existence of a material gap is quite common in complex systems. If a material gap exists, i.e. if the catalyst composition changes during reaction, the existence of a reaction gap has to be suspected. Do the reactants take part in the change of the catalyst composition? How important is such a stoichiometric reaction?

In order to obtain a high surface area, real catalysts are either highly dispersed on a support or have a high inner surface formed by pores. Transport properties for matter (reactants and products) and heat from and to the active sites are often decisive but their influence is difficult to separate from the properties of the elementary catalytic reaction. Model catalysts can be prepared undispersed and free of pores. Even if the surface structure and morphology changes under reaction conditions, the bulk remains free of pores. The catalytic reaction can therefore be studied without transport limitations. The influence of polycristallinity, dispersion and pores can then be introduced step by step in a controlled way [10].

Here, we review the model catalysis approach applied to the investigation of the catalytic dehydrogenation of ethylbenzene (EB) to styrene (St) which industrially is performed over potassium-promoted iron oxide catalysts. With more that 20 mio t per year worldwide, this reaction belongs to the 10 most important catalysed organic reactions. The reaction (fig. 1) is endothermic (ΔH=125 kJ/mol) and has to be run at high temperature, typically 870 K. The

pressure is 1 bar but since steam in excess (molar ratio EB:H_2O between 1:6 and 1:10) is added to the reactant mixture, the partial pressure of EB is correspondingly lower. The steam is considered to transport the heat, to counteract coking by the coal gasification reaction and to act as a diluent so that the equilibrium is shifted towards the product side.

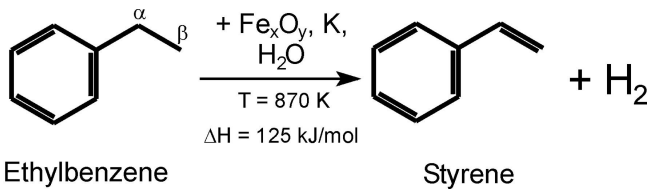

Figure 1: The dehydrogenation of ethylbenzene (EB) to styrene (St) is endothermal. Technically it is performed at 870 K over potassium-promoted iron oxide catalysts in the presence of steam in excess.

The catalyst is complex. Since the divalent Fe^{2+} and the trivalent Fe^{3+} state are similarly stable, there exist several stable or metastable oxide phases. The reaction atmosphere is reducing due to the H_2 liberated in the reaction. This influences the catalyst phase during reaction. Addition of K adds several stable or metastable ternary KFe_xO_y phases to the zoo of possible catalyst phases. Surface science can contribute to the identification of substrate phases. The interaction of steam with the catalyst, especially with K, and its influence on the catalyst phase has to be considered. Also here, surface science contributes to our understanding.

The reactant ethylbenzene C_8H_{10} is also fairly complex. However, in agreement with chemical knowledge, surface science tells us that the aromatic benzene ring is a comparatively stable and well-defined unit as is the ethyl group where the dehydrogenation has to occur. Deuteruim exchange occurs readily at the α-position of the ethyl group of EB and much faster than at any other position in EB, especially the β-position[11]. Therefore dehydrogenation will start at the α-position and the structure of the active site should fit to interact at this position.

As with most catalytic processes involving organic compounds, a major problem is the formation of carbonaceous deposits (here shortly termed ‘coke’) as a result of side reactions leading to further or even full dehydrogenation of adsorbates. The formed coke covers the active surface and deactivates it. As mentioned, the added steam is believed to counteract coking by the coal gasification reaction. Coke is not necessarily inactive but its role as catalyst is not well established. Surface science turns out to be able to shine some light on the coking process.

Since especially the thermodynamically most stable iron oxide phase, hematite α-Fe_2O_3, is an electrical insulator, the application of surface science techniques using charged particles is difficult. Therefore, an important reason for the choice of this catalytic system was that thin FeO, Fe_3O_4 and Fe_2O_3 films of single crystalline equality can be grown epitaxially on single crystalline Pt supports. It turned out that films about 10-20 nm thick still have sufficient electrical conductivity. Thin films have further advantages: The oxide film can easily be renewed if destroyed or contaminated, it consists of a limited and well know amount of “bulk” material which is an advantage if reactions with the bulk material are suspected. Further, the time-consuming and annoying procedure of removal of bulk contaminants segregating at the surface is avoided. Thin film growth and characterization is the domain of surface science.

The basic idea of model catalysis as we apply it is to prepare well defined model catalyst samples and to characterize their surface structure and composition as well as their adsorption-desorption properties for the relevant gases. This is described in chapter 2. Then the samples are transferred under vacuum into a reactor which allows to determine the catalytic properties (conversion, selectivity, deactivation behaviour) in-situ under realistic temperature and pressure conditions. After that, the samples are transferred back into the main UHV chamber for post-reaction analysis. The reactivity studies are the subject of chapter 3. The conclusions drawn for the catalytic system considered here and more generally for model catalysis as a whole are presented in chapter 4.

2. MODEL CATALYST PREPARATION AND CHARACTERIZATION

2.1 Instrumentation

Three ultrahigh vacuum (UHV) systems were used, all with a base pressure in the low 10^{-10} mbar range. All are equipped with a high-pressure chamber and a sample transfer system. The high-pressure chamber is separated from the main chamber by a gate valve and serves also as a load-lock. The arrangement is schematically shown in fig. 2. One of the systems contains a single-crystal micro-flow reactor integrated into the high-pressure chamber which will be described in more detail in section 3.2. All systems contain facilities for sample preparation (sample heating and cooling, sputter gun, evaporators, gas inlet systems) and an optics for low-energy electron diffraction (LEED). As specialties, one system contains equipment for thermal desorption mass spectroscopy (TDS) and a spectrometer for Auger electron spectroscopy (AES) and the sample can be transferred into a further chamber with a photoelectron emission microscope (PEEM) and an ion scattering spectrometer (ISS). The second system contains a scanning tunneling microscopy (STM) system and the third one a spectrometer for X-ray and ultraviolet photoelectron spectroscopy (XPS, UPS).

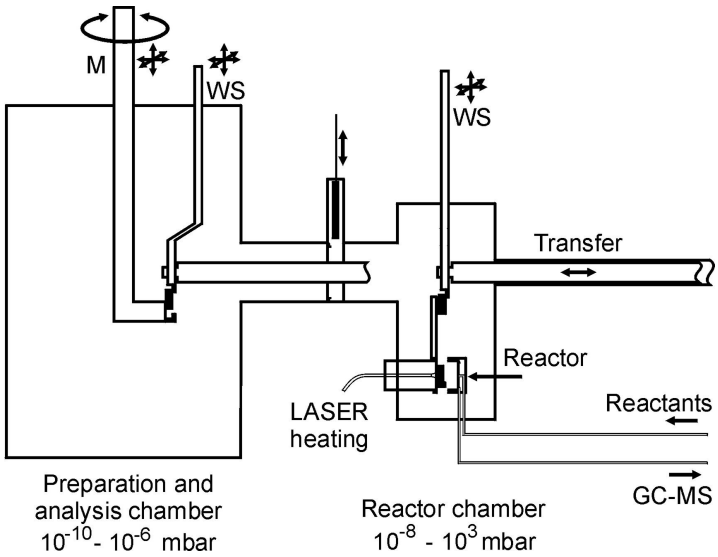

Figure 2: Experimental setup, schematic, consisting of the preparation and analysis chamber working at ultrahigh vacuum and the reactor chamber, working at pressures up to 1 bar. The sample on its support (figure 3) is moved by a magnetically coupled transfer rod. The transfer between the rod ond the manipulator M or the reactor is accomplished by wobble sticks WS.

Samples are mounted on sapphire transfer supports as shown in fig. 3. Sapphire is used because it is chemically inert, mechanically stable and has unique thermal properties. At low temperature, its heat conductivity is high and allows cooling while it is a thermal insulator at

higher temperature which allows annealing without high thermal losses. The four screws have electric contact from behind when inserted into the sample station of the manipulator or the reactor. Two of them are used for sample mounting and two for a thermocouple. Below the sample, there is a hole in the sapphire support so that heating is possible from behind using either electron bombardment or laser irradiation.

NEXAFS measurements were performed in a cooperation project at the former synchrotron storage ring BESSY-1 [12].

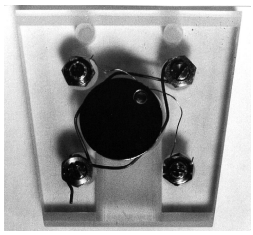

Figure 3: Pt substrate sample on sapphire support. The screws are contacted from behind to the manipulator or reactor when inserted. Two screws (lower left and upper right) are used to fix the sample on the support, the others for a K-type thermocouple. The support has a hole below the sample for heating by electron bombardment or laser irradiation from behind.

2.2 Preparation

The preparation of Fe_xO_y and KFe_xO_y films is reviewed in [13] and is illustrated schematically in fig. 4. Iron is evaporated at room temperature on a clean single crystalline Pt(111) substrate. Also Pt(001)[14], Ru(0001)[15,16] and Cu(111) [17] substrates can be used. When this layer is exposed to 10^{-6} mbar O_2 at 870 – 1000 K, it oxidises to a thin oxide layer with the characteristics of FeO(111). Depending on temperature and substrate, its maximum thickness is 1 – 4 Fe-O bilayers. It is always terminated by oxygen. Further iron deposition and oxidation at 870 K results in the growth of Fe_3O_4(111) islands on and into the FeO layer. Eventually they coalesce into a closed film. Post-annealing this film at 1000 K improves its long-range order. Films used as model catalysts were grown to a thickness of 10 – 20 nm. The iron-oxygen phase diagram in fig. 4 shows that Fe_2O_3 should be the thermodynamically stable phase for $p(O_2)=10^{-6}$ mbar and T<1050 K. Obviously, its formation is kinetically hindered. Therefore, higher oxygen pressures between 10^{-4} and 1 mbar have to be applied to convert the Fe_3O_4 films into α-Fe_2O_3 within a reasonable time.

In order to produce K-promoted model catalyst films, K is deposited on Fe_3O_4 or Fe_2O_3 films using a SAES getter source, followed by annealing in vacuum or at $p(O_2)=10^{-6}$ mbar. The most stable K-Fe-O phases are the K-rich $KFeO_2$ (K-ferrite) and the K-poor $K_xFe_{22}O_{34}$ with x=2 (K-β-ferrite) or x=4 (K-β''-ferrite). $K_xFe_{22}O_{34}$ has a hexagonal layer structure which can be considered as a sequence of spinel-like blocks $-(O_4\text{-}Fe_3)_3\text{-}O_4$- etc. as in Fe_3O_4, separated by -Fe-$K_{x/2}$O-Fe- layers. Lower K-contents (x<2) can be achieved either by increasing the thickness of the spinel blocks, thus continuously approaching the pure Fe_3O_4, or by a decrease in the occupation of the potassium sublayers in analogy to the structure of corresponding alumina clay minerals. Because of the similarity of the spinel blocks with the Fe_3O_4 spinel structure, the lattice constant of the $K_xFe_{22}O_{34}$(0001) and Fe_3O_4(111) surfaces are almost identical and epitaxial growth is easy. $KFeO_2$ is tetragonal without any layered character and does not fit with the lattice of Fe_3O_4. In its bulk, the K, Fe and O atoms are quite homogeneously distributed.

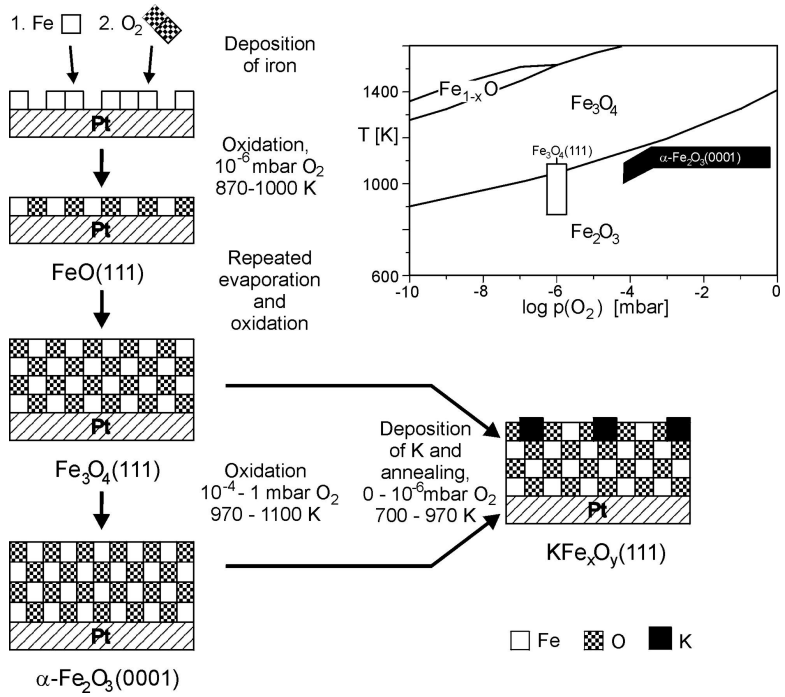

Figure 4: Preparation of binary Fe_xO_y films and ternary KFe_xO_y films. Included is the Fe-O phase diagram [18].

2.3 Characterization: Surface structure

Figure 5 shows the LEED patterns, STM images and surface structure models of those model catalyst layers which form ordered surfaces. The hexagonal oxygen layers are very similar in all cases with O-O distances varying only between 0.290 nm in Fe_2O_3, 0.296 nm in Fe_3O_4 and $K_xFe_{22}O_{34}$ and 0.304 nm in bulk FeO. The thin FeO layers on Pt have expanded lattice constants. The strong differences in the LEED patterns and the STM images result therefore from the different arrangement of the Fe atoms between the oxygen layers. Typical for the quite thin FeO(111) layers (shown is the pattern of a film only one Fe-O bilayer thick) are the satellite patterns around the integral order spots in LEED and the Moiré pattern of the STM image. Both are due to the low film thickness and the misfit between the Pt(111) and the FeO(111) lattice. The satellite spots result from multiple scattering involving the Pt and FeO lattice. The Moiré pattern reflects the different positions of the Fe atoms on the Pt lattice, periodically changing between on-top, bridge and threefold hollow site positions. All three kinds of sites occur in the shown structure because the FeO layer is rotated with respect to the Pt substrate. Photoelectron diffraction [19] and STM studies [20] have shown that the surface is oxygen terminated. However, the bright dots in STM reflect the positions of the Fe atoms underneath which show both unoccupied and occupied levels near the Fermi level [20]. For details of the structure see ref. [13].

The $Fe_3O_4(111)$ surface has a threefold symmetry. Mostly, however, two domains rotated by 60° with respect to each other are equally distributed so that the LEED pattern has sixfold symmetry. As for FeO, the STM image reflects the surface unit cell. Again, the bright spots correspond to surface Fe atoms. They are quite clear on $Fe_3O_4(111)$ because this surface Fe forms the top layer as proven by a LEED structure analysis [22] and indicated in the model.

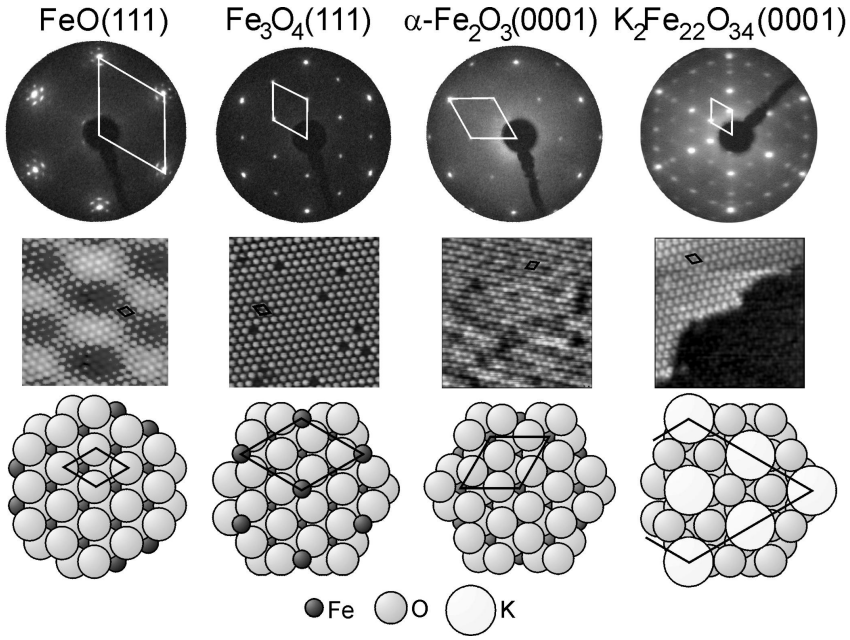

Figure 5: LEED patterns, STM images and structure models of ordered binary Fe_xO_y films and the only long-range ordered ternary $K_xFe_{22}O_{34}$(0001) film (x»0.67). The structure models for the binary films result from structure analysis, that of $K_xFe_{22}O_{34}$ is hypothetical but it reflects the surface composition as deduced from XPS measurements [21].

The surface unit cell of α-Fe_2O_3(0001) is again different. The STM image is again formed by Fe derived spots but the contrast is lower than on Fe_3O_4. The reason is that the surface is oxygen-terminated or possibly even hydroxylated as a LEED structure analysis has shown [23].

Depending on the amount of deposited K and the annealing temperature, different ternary K-Fe-O compounds are formed. Already at 300 K, the deposited K diffuses into the bulk and at 700 K, the K-rich $KFeO_2$ phase forms uniformly as concluded from quantitative XPS results [21]. It has, however, no long-range order and no LEED patterns are formed. STM imaging is difficult and only possible on a very thin (2 nm) film because the compound is an insulator. The film is rough and atomic resolution is not achieved [24]. When annealing between 800 and 900 K, potassium is slowly removed from the film (the speed increases strongly when water is present) in the way that a $KFeO_2$ layer of decreasing thickness remains at the surface while the underlying film converts to $K_xFe_{22}O_{34}$. The $KFeO_2$ disappears completely at 970 K and a $K_xFe_{22}O_{34}$ layer is left. The XPS results [21] suggest that the surface is terminated by a complete Fe-K-O layer while the bulk contains less potassium, corresponding to about $x \approx 0.67$. This is the only KFe_xO_y layer with good long-range order. Its LEED pattern and STM image are shown in fig. 5.

2.4 Characterization: Adsorption properties

A great deal of work has been spent on the determination of the surface structure using LEED spot intensity measurements in combination with dynamic structure analysis calculations [14,22,23], on the determination of the kind of adsorbed species (molecular or dissociated) after exposure to EB [25], St [26] and H_2O [27] using UPS, on the adsorbate orientation using NEXAFS [12] and on the energetic and kinetic data for adsorption and desorption using TDS [28] and isosteric methods [26]. The collected knowledge for EB and St is summarized in fig. 6.

The FeO film is O-terminated. The first Fe layer is relatively deep below this O-layer (-0.068 nm [19] or 0.062 nm [20]). Also Fe_2O_3 is O-terminated but according to the best-fit structure [23], the first Fe layer is only 0.046 nm below the surface O-layer. In contrast, Fe_3O_4 is Fe-terminated. The Fe atoms are +0.038 nm above the first O-layer [22]. This has a decisive influence on adsorbate orientation and interaction. UPS shows that all adsorbate states of EB and St at room temperature and below are molecular (for decomposition behaviour see below). NEXAFS shows for FeO that EB and St adsorb strongly tilted from the beginning. The only adsorbate state is a weakly bound physisorbed state. Although there is no direct evidence for island formation of the adsorbate, we believe therefore that the adsorbate-substrate interaction is so weak that adsorbate-adsorbate interaction dominates. As characteristic for condensed aromatics, this interaction is assumed to occur via the π-orbitals of the benzene ring so that the molecules get tilted. In contrast, both EB and St adsorb almost flat on Fe_3O_4 and Fe_2O_3, at least for low coverages. Near saturation, tilting increases due to increasing adsorbate-adsorbate interaction. Flat adsorption correlates with the existence of chemisorbed γ-states which saturate before a second, physisorbed layer forms. Chemisorption is much stronger on Fe_3O_4 than on Fe_2O_3, and it is stronger for St which has a conjugated π-system extending also over the ethyl group, at least if it adsorbs in a planar configuration.

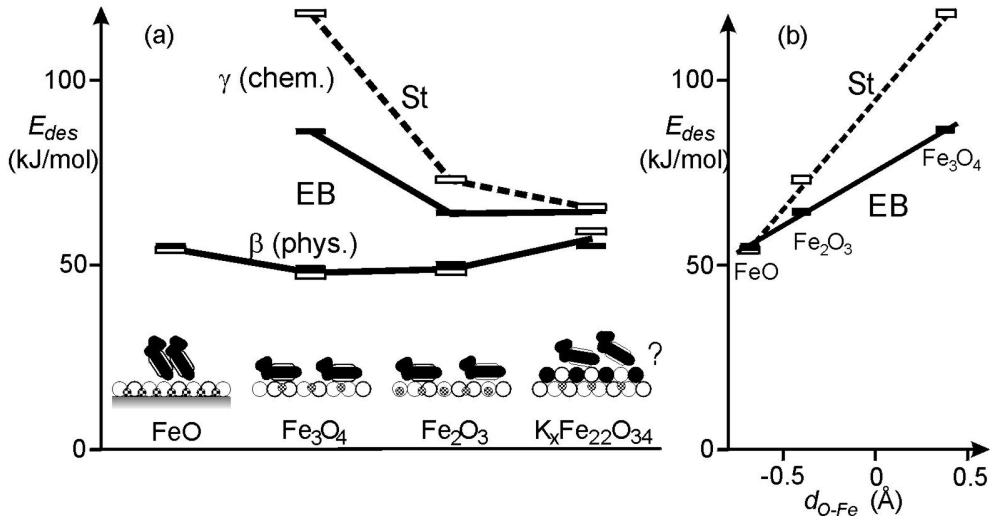

Figure 6: Energetic and structural results for EB (filled symbols) and St (open symbols) adsorption on different substrate films. (a) Desorption energies from TDS [29] for chemisorbed (g) and physisorbed (b) species and adsorbate arrangement at low coverages of the initially adsorbing species (b on FeO, g on the others). Shown is adsorbed EB, the arrangement for St is similar. Adsorbate structure for Fe_xO_y from NEXAFS measurements [12]. The arrangement on $K_xFe_{22}O_{34}$ is hypothetical. (b) Dependence of the desorption energy for the initially adsorbing species on the position of the first iron layer relative to the first oxygen layer.

UPS measurements for EB on Fe_3O_4 in adsorption-desorption equilibrium show that saturation of the chemisorbed γ-state corresponds to one EB molecule on two Fe surface sites. This corresponds to only about 83 % of a close-packed adlayer assuming a flat adsorbate configuration (Van-der-Waals area of EB ~0.5 nm^2). The physisorbed first β-layer on FeO, however, saturates at a full monolayer which rules out a correlation of the adsorbate with the surface structure [27].

These results prove that chemisorption is dominated by the interaction between the strongly polarizable π-system of the adsorbate which represent a soft base [30] and the acidic Fe ions. This is highlighted by fig. 6 b which gives the dependence of E_{des} for the initially adsorbing species (β for FeO, γ for Fe_2O_3 and Fe_3O_4) on the Fe-layer position with respect to the O-layer. On Fe_2O_3, the Fe-layer is relatively deep below the O-layer but the molecules can obviously still "feel" it and arrange in a flat chemisorbed state. Although the Fe-layer is not much deeper on FeO, the interaction is too weak to compete with the Van-der-Waals interaction between the adsorbates.

For the $K_xFe_{22}O_{34}$ film, a structure analysis does not exist. The quantitative XPS results [21] are compatible with a termination by a Fe-K-O layer as in the bulk of $K_2Fe_{22}O_{34}$. In this case, the first Fe atoms are below the O atoms of the top layer and an interaction with the adsorbate would be weak. On the other hand, interaction may include surface K ions, but as long as a structure analysis is missing, any adsorption model is speculative. The existence of a chemisorbed state which preceeds physisorption and has similar binding energies as on Fe_2O_3 suggests that the binding situations on these two surfaces are similar. The difference of the binding energies for EB and St has disappeared.

3. CATALYTIC CHARACTERIZATION

3.1 Low and medium pressure reactivity measurements

The first reactivity measurements were performed on unpromoted model catalysts using mass spectrometric analysis in the main UHV chamber. A mixture EB:H_2O=1:5 at a total pressure of 3.5×10^{-6} mbar was applied. It turned out that well ordered Fe_2O_3 hematite samples with sharp spots and low background in the LEED pattern were quite inactive while poorly ordered samples with broad spots and high background clearly showed conversion. Typical mass spectrometer traces are presented in fig. 7 (from [31]) The sample was kept at 873 K, water was admitted at t=0, EB about 20 – 30 s later. On a poorly ordered active Fe_2O_3 film, deactivation was observed after several such cycles, going along with indications for reduction to Fe_3O_4 in the LEED pattern. Also carbonaceous deposits were detected by photoelectron emission microscopy (PEEM). On magnetite Fe_3O_4 samples, activity could not be detected, irrespective of the surface order.

In a first attempt to bridge the pressure gap, medium pressure batch reactor experiments were performed. The high pressure chamber (fig. 2, at that time without reactor) was used as batch reactor cell. For mass spectrometric analysis, a bypass line with a dosing valve was mounted between the high pressure chamber and the UHV analysis chamber. The gas mixture (EB:H_2O=1:10, total pressure 0.6 mbar) was admitted and after about 10 min, sample heating was started. After a few minutes, the reaction temperature was reached. Fig. 8 shows that styrene and hydrogen evolution goes along with ethylbenzene consumption. Again, activity increases with the degree of disorder of the starting Fe_2O_3 film. The most active film was deactivated after about 30 min. PEEM showed complete coverage by coke deposits. In AES, carbon was visible and after its removal by a mild oxidation cycle, LEED showed a mixture of the patterns of Fe_2O_3 and Fe_3O_4, confirming catalyst reduction during the experiment.

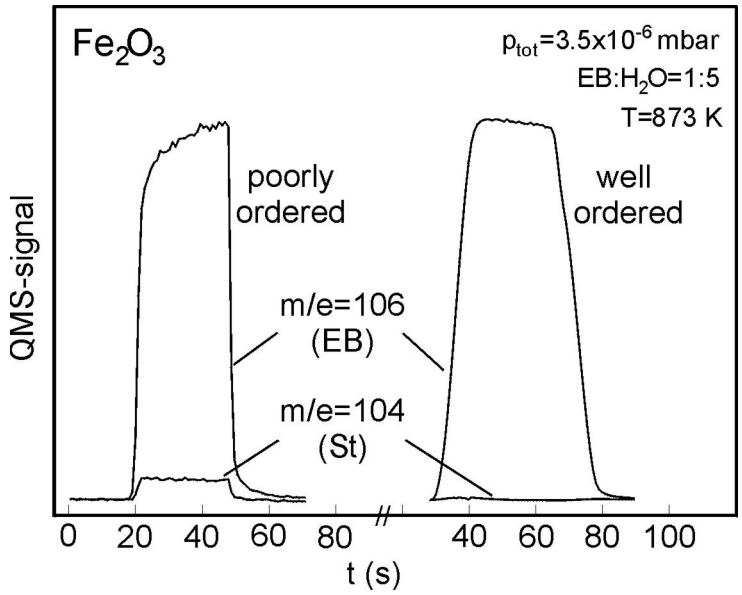

Figure 7: Mass spectrometer traces for EB and St under low pressure reaction conditions as indicated over poorly ordered and well ordered Fe_2O_3 samples. Water was admitted at t=0. The traces reflect the periods of EB admission.

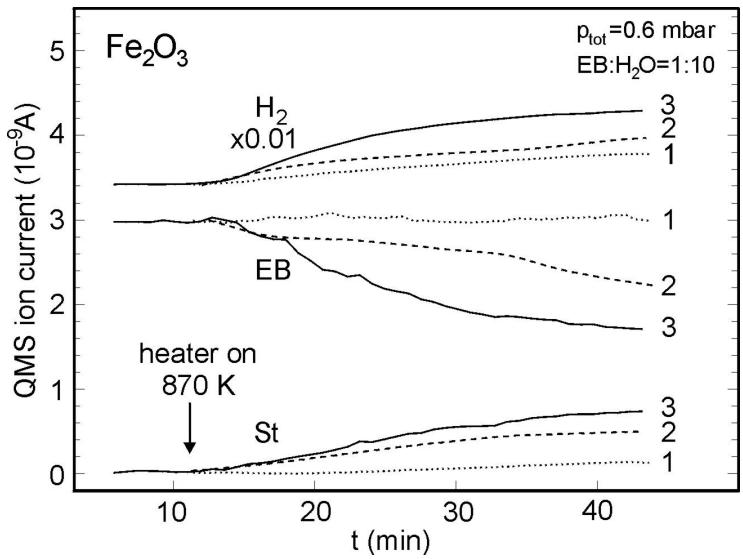

Figure 8: Mass spectrometric analysis of a batch reactor experiment at intermediate pressure conditions for three Fe_2O_3 model catalysts with differing surface quality. (1) well ordered, (2) intermediate order, (3) poorly ordered.

Coke formation was weaker on the film with intermediate activity and lowest on the inactive film. This is a hint that the product molecule St is mainly responsible for coking.

This is confirmed by UPS investigations which yield information about the adsorbed species (molecular or dissociative). They are reviewed in [26]. At temperatures below 400 K, adsorption of EB on FeO and Fe_3O_4 is molecular and completely reversible. The adsorbed amount depends only on the pressure and the temperature. The EB can be desorbed thermally without any decomposition products. The situation is different for St. When a St layer is condensed on FeO at low temperature and heated off again, a submonolayer amount of a residue with spectral features of polystyrene remains irreversibly on the surface. The

thickness of this layer increases upon further condensation-desorption cycles. Since the interaction of St with the oxygen terminated FeO substrate is weak (no chemisorption, see fig. 6) so that the substrate influence is minimized, this shows that polymerization as a reaction channel open for St but not for EB is quite effective. Due to the existence of surface Fe, interaction of EB and St with Fe_3O_4 is much stronger and chemisorption is observed. In the case of St, also here an irreversibly adsorbed species is found which, however, does no more show the spectral features of polystyrene but seems to represent decomposition products. In a St atmosphere, the coverage of this species is continuously growing. A similar species was also observed in an investigation on Pt where the annealing behaviour was studied in detail [32]. With increasing temperature, decomposition proceeds further and beyond 700 K, only a graphitic coke layer is left.

Under high pressure and temperature conditions of catalysis, it is likely that both EB and St partly decompose but the UPS studies in UHV have shown that coke formation by St is by far more effective because it offers formation of oligomers as a first step in the reaction route. Oligomers as larger entities are less easily desorbed. Instead, they decompose at the reaction temperature. Therefore, the product molecule St is mainly responsible for coking.

Experiments as in fig. 8 were also performed using Fe_3O_4 model catalysts, again without measurable activity.

The low and medium pressure conversion experiments show that meaningful conversion measurements can be performed over single crystal samples with a surface area as small as 0.5 cm^2. They confirm that Fe_2O_3 is clearly more active than Fe_3O_4. Deactivation of Fe_2O_3 goes along with reduction and coking and defects are necessary for high conversion.

3.2 In-situ micro-flow reactor

In order to be able to apply still higher pressures and also to simulate real catalysis conditions more quantitatively, the micro-flow reactor shown in fig 9 was implemented. The reactor is constructed on a 70 mm od flange which carries the feedthroughs for the thermocouple and for two fiber rods which are used for coupling in laser radiation for sample heating. Two flexible capillaries are connected to the reactor cap, one for admission of the reactant gas mixture and one as product gas outlet. When the reactor cap is retracted (fig. 9 a), the sample on the sapphire support can be inserted into the reactor using a wobble stick. After retraction of the wobble stick, the cap is closed (fig. 9 b) and the arrangement represents a stagnation point reactor with a total volume of only about 4 ml. Due to the small distance between sample and cap (typically 1 mm), the gas volume in contact with the sample is much smaller (~0.05 ml). Under typical flow conditions (p=1 bar, 25 ml min^{-1}), the contact time is only about 0.12 s.

The sample is heated from behind by radiation from two diode laser stacks with a total power of max. 100 W. This is necessary to reach a reaction temperature of 870 K under flow conditions.

Product analysis is achieved with a gas chromatograph equipped with an ion trap mass detector (GC-MS). The used setup is optimized for separation and analysis of EB, St, toluene and benzene but not suitable for smaller hydrocarbons, CO_2, CO and H_2. GC analysis is cyclic and can be repeated every three minutes.

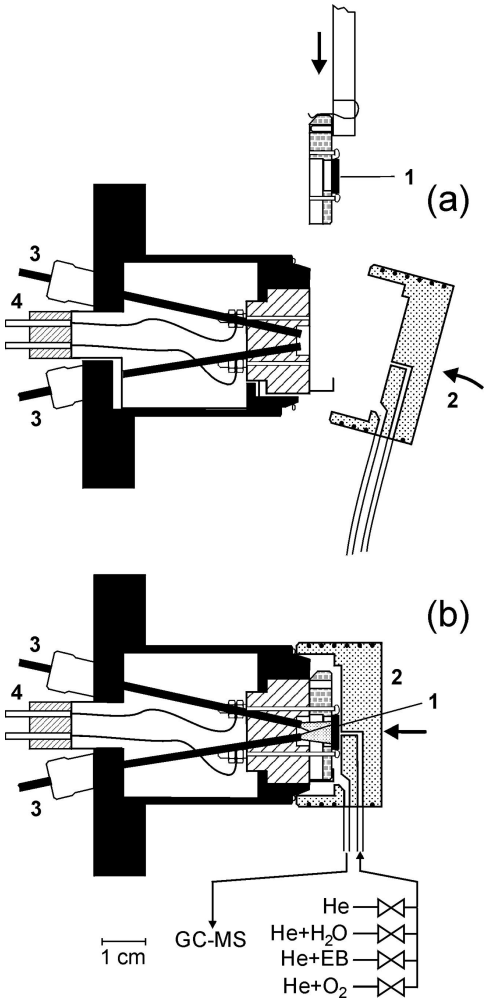

Figure 9: Stagnation point micro-flow reactor for model catalysis at high pressure. 1: sample on sapphire support; 2: reactor cap; 3: fiber rods for coupling in laser irradiation; 4: thermocouple feedthrough. (a) during insertion of the sample on a wobble stick, reactor cap withdrawn. (b) reactor cap closed, gas admission and analysis lines schematically shown.

Since surface characterization cannot be performed during reactivity measurement at high pressure, the procedures of sample transfer, gas admission and heating before reaction which takes about 20 min, and the quenching and evacuation after reaction are of decisive importance. After transfer, the reactor cap is preheated and outgassed under vacuum at 670 K, then the chamber is backfilled with N_2 and a flow of pure He (K-promoted samples) or He with admixture of H_2O (Fe_3O_4) or H_2O and O_2 (Fe_2O_3) is admitted to the reactor. The sample is heated to the reaction temperature (870 K), the flow composition is switched to the reaction conditions (table 1) and the GC measurement is started. After the reactivity measurements, the reactive gases EB, H_2O and O_2 are switched off and the sample is cooled in a flow of pure He to 600 K within less than 60 s. When 500 K is reached, the reactor chamber is evacuated and the sample transferred for post-reaction analysis.

In order to make sure that the surfaces are not changed by these procedures, a Fe_2O_3 sample was exposed to a heat-up and cool-down cycle without reaction. The surface turned out to be clean and it showed the characteristic LEED pattern. Further, after reactivity studies, cool-down and post-reaction characterization, samples were transferred back and the reaction was restarted. They showed the same catalytic activity as before cool-down.

Post-reaction AES analysis showed always that the samples were at least partially covered by carbonaceous deposits ('coke') and LEED showed only diffuse background intensity which indicates disorder. In order to analyse the substrate phase, the coke was removed by one or several mild thermal programmed oxidation (TPO) cycles. The sample was heated in 10^{-6} mbar O_2 at a rate of 5 K s^{-1} to 1000 K [33]. At this low pressure, reoxidation is kinetically hindered so that the oxidation state of the substrate is not changed [18].

Reaction conditions	p (mbar)	Molar ratios
Normal	p(EB)=3.3	EB : H_2O
	$p(H_2O)$=33	1 : 10
Reductive	p(EB)=3.3	--
Oxidative	p(EB)=3.3	EB : H_2O : O_2
	$p(H_2O)$=33	1 : 10 : 0.5
	$p(O_2)$=1.7	

Table 1: Partial pressures and molar ratios of reactive gases in the gas feed for the used standard reaction conditions. The rest to the working pressure of 1 bar is He. The standard reaction temperature is 870 K, the standard total flow 25 ml min^{-1}.

Table 1 lists the standard reaction conditions used. Normally, H_2O in excess is added in the technical process. In order to check the role of water, also experiments without water (reductive) were performed. In oxidative conditions, some oxygen was added.

3.3 Unpromoted Fe_2O_3, Fe_3O_4

For hematite (Fe_2O_3) as starting surface, the dependence of the St conversion rate on the time on stream for the normal reaction conditions (EB:H_2O = 1:10) is shown in fig. 10a [34,35]. The initial rate decays within about 70 min by about one order of magnitude. The experiment was repeated with freshly prepared hematite substrates (different symbols) and stopped at the positions A, B and C. Post-reaction analysis showed that the substrate was only moderately coked at A. The intensity ratio of the main Auger peaks of C and Fe is I_C/I_{Fe}=1.1. After one TPO cycle, the LEED pattern of Fe_2O_3 was recognizable but the spots were diffuse, indicating disorder. At B, coking was strong (I_C/I_{Fe}=3.6) and 3 TPO cycles were necessary to remove it. After that, both the patterns of Fe_2O_3 and Fe_3O_4 appeared indicating that the substrate was partially reduced. Most likely, reduction had started from the surface, leaving a disordered Fe_3O_4 layer since in-depth reduction is kinetically limited by oxygen out-diffusion. The phase separation into the ordered Fe_2O_3- and Fe_3O_4-domains seen in LEED happened probably during the TPO cycles which involve heating. At C, the coking had not increased (I_C/I_{Fe}=3.4) but LEED after 3 TPO cycles showed complete reduction to Fe_3O_4. Deactivation is thus related with substrate reduction or coking or both.

Fig. 10b shows the corresponding measurement with Fe_3O_4 as starting surface [36]. The initial rate is clearly lower than for Fe_2O_3 but it decays to the same final value and post-reaction analysis at D shows the same final state: coked Fe_3O_4. The lower initial activity compared to Fe_2O_3 and its further decay by coking prove that the deactivation of Fe_2O_3 in fig. 10 a in fact is due both to substrate reduction and to coking.

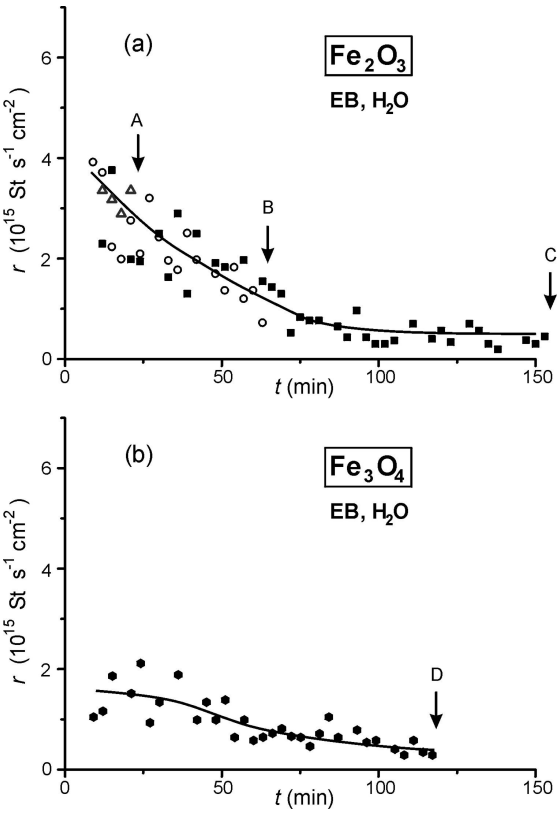

Figure 10: (a) St conversion over Fe_2O_3 under normal conditions (see table 1); three measurements, finished at A, B, C for post-reaction analysis. (b) St conversion over Fe_3O_4 under normal conditions. Post-reaction analysis at D.

During reduction of Fe_2O_3, oxygen is liberated. It could therefore be possible, that the dehydrogenation in this period (approximately until B in fig. 10 a) is not catalytic according to the equation

$$C_8H_{10} \rightarrow C_8H_8 + H_2, \quad (1)$$

but stoichiometric, involving reduction of the substrate:

$$C_8H_{10} + 3Fe_2O_3 \rightarrow C_8H_8 + 2\,Fe_3O_4 + H_2O. \quad (2)$$

Since the thickness of the used model catalyst film is known, the amount of liberated oxygen assuming complete reduction to Fe_3O_4 can be calculated and compared to the amount of St (which equals the amount of H_2) produced during this period. It turns out that the amount of St exceeds the amount of available oxygen by at least a factor of 700. The reaction on Fe_2O_3 is thus essentially catalytic.

It was often argued that the water could take an active part in the reaction, e.g. by reoxidation of the substrate if lattice oxygen would be removed together with adsorbed hydrogen in form of H_2O (Mars-van Krevelen mechanism). The time dependence of the conversion rate was therefore also measured without water in the feed. It is shown in fig. 11 (lower curve) [34,35]. The initial rate is very similar to that with water. Although the presence of water traces cannot be ruled out, this makes it unlikely that water is involved in the catalytic reaction on clean Fe_2O_3. Also the deactivation behaviour seems similar. However, interruption at E and surface analysis revealed heavy coking (I_C/I_{Fe}=5.3) and oxygen depletion. Even after several TPO cycles, no LEED pattern could be restored. At F, the Auger measurement showed only carbon. After many TPO cycles, a weak pattern of clean Pt(111) reappeared. Since oxidation

reproduced Fe_2O_3, it was concluded that Fe had not been lost but coalesced into metallic islands or alloyed with the Pt substrate. The iron had thus been reduced to metallic Fe^0 at F. The final conversion rate is characteristic for carbon. Since it has the same magnitude as the final rates in fig. 10 a and b, it was supposed that also there the active species in the final state was coke and not the oxide below.

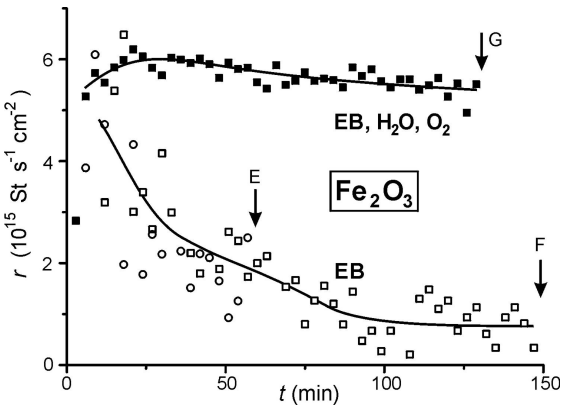

Figure 11: Lower curve: St conversion over Fe_2O_3 under reductive conditions (see table 1) without water in the feed; two measurements finished at E, F for post-reaction analysis. Upper curve: St conversion over Fe_2O_3 under oxidative conditions (see table 1) with O_2 added to the feed. Post-reaction analysis at G.

In a further experiment, it was tried to prevent reduction and coke accumulation by addition of oxygen to the feed [34,35]. The upper curve in fig. 11 shows the result for the oxidating conditions of table 1 ($EB:H_2O:O_2 = 1:10:0.5$). In fact, the conversion rate stabilizes at a value even higher than the initial rates without O_2 (lower curve and fig. 10 a). Assuming the same reaction mechanism with and without O_2, this suggests that the first measured points without O_2 already represent slightly deactivated surfaces. Post-reaction analysis at G reveals only slight coking ($I_C/I_{Fe}=0.8$) and LEED after only one TPO cycle shows, as expected, the pattern of unreduced but disordered hematite.

The equilibrium thermodynamics of the $Fe\text{-}O_2\text{-}H_2\text{-}H_2O$ system has been investigated experimentally by Muan [37]. Calculations based on thermodynamic data confirm the results [38]. For the reaction temperature of 870 K, Fe_2O_3 is reduced in presence of H_2. Without H_2O, this proceeds to metallic Fe^0 while the presence of H_2O limits reduction to Fe_3O_4. This confirms that the hydrogen produced during EB dehydrogenation is responsible for the observed reduction effects. It also confirms that the role of H_2O is not only to balance coke formation by the coal gasification reation but also to limit reduction beyond the magnetite phase, as observed. The thermodynamic considerations showed also that hematite reduction can be prevented by addition of oxygen. The necessary minimum amount correspond to only very slightly less than that necessary for the stoichiometric water formation reaction $H_2 + ½ O_2 \rightarrow H_2O$.

The steady state conversion rate after a 50 min reaction period decreases when the oxygen partial pressure is reduced. An estimation shows that the optimal value as used in fig. 11 (upper curve) corresponds to the oxygen necessary for oxidation of the hydrogen originating from the EB dehydrogenation and from coking reactions as well as for oxidation of the coke itself [36]. For higher oxygen flow rates total oxidation becomes dominant.

The observed reduction of the hematite to magnetite agrees with observations on technical catalysts [39,40]. However, the high initial rate associated with clean hematite was not

observed before. Obviously it was hidden in the start-up and equilibration periods. It is therefore likely that the investigations on technical catalysts observed only the fully deactivated state. An exception is a recent measurement on pressed Fe_2O_3 powder pellets under technical conditions (1 bar, pure EB + H_2O atmosphere, EB:H_2O=1:6) where the initial high conversion rate decreased within the first minutes on stream by a factor of about 8 to10 [34]. Upon addition of oxygen (EB:H_2O:O_2=1:6:0.4), the steady state conversion did not rise to the initial value but could be enhanced by a factor of three. The concentration of O_2 was obviously not sufficient for full prevention of reduction and coking.

In the low and medium pressure experiments with p(EB)+p(H_2O) between 3.5×10^{-6} and 0.6 mbar, there was clear evidence that defective Fe_2O_3 surfaces are catalytically more active than well ordered ones. In the high pressure experiments p(EB)+p(H_2O) = 36 mbar, no indications for a defect dependent initial activity was observed but post-reaction analysis showed always that disorder had formed during reaction. Formation of disorder is not unexpected because of the observed reduction which implies outdiffusion of oxygen and nucleation of magnetite with its different crystal structure. Also when O_2 is added so that no net reduction occurs, surface reduction-oxidation processes may occur dynamically under reaction conditions. While at low and medium pressures the formation of defects is slow enough so that the influence of initial surface disorder is clearly visible, defect formation at high pressure may be so fast due to the more violent reaction conditions that it has happened within the first minutes and may at most influence the first GC data point after gas admission. Indeed, the first data points sometimes indicate lower conversion but this is more likely due to a temporary temperature decrease upon admission of EB. The importance of defects for the mechanism of the catalytic reaction can thus only be deduced from low and medium pressure experiments.

Deactivation reduces the activity considerably but the final activity is not zero. Most likely, this final activity is due to the carbonaceous deposits. Certain forms of carbon are active catalysts in oxidative dehydrogenation of EB [41,42]. If no oxygen is added and after reduction of the substrate, the only source of oxygen is the water which may supply oxygen according to the dissociation equilibrium at the reaction temperature or to the coal gasification reaction which may supply CO. Post-reaction Auger analysis also revealed oxygen at the surface in this case. Without water, even this source of oxygen is missing. Consequently, no oxygen was visible in AES. However, the final activity in fig. 10 a and fig. 11 (lower curve) is the same, independent of the presence of water. The mechanism over the deactivated catalyst is thus not yet clear.

3.4 K-promoted KFe_xO_y

Fig. 12 shows representative conversion rate measurements for K-promoted model catalysts with different K-content [36]. A relative measure of the K-content is the I_K/I_{Fe} Auger intensity ratio. The $K_xFe_{22}O_{34}$ film used in Fig. 12a had $I_K/I_{Fe}\approx2.3$ which is not far from the value of the 2×2 surface ($I_K/I_{Fe}\approx2.7$, x≈0.67, see section 2) . The initial conversion rate is near to that of the unpromoted film (also shown for comparison in fig. 12a) but the deactivation is much slower. Post-reaction analysis showed only weak coking (I_C/I_{Fe}=0.5) and a moderate reduction of the K-content to $I_K/I_{Fe}\approx1.8$.

In the industrial process, deactivated catalysts are regenerated by running the reactor without EB but only steam in the feed (“steaming”). This treatment was simulated on the model catalyst used in Fig. 12a by transferring it again into the reactor and running it for 15 min without EB but with the same flux of water as before. Then the EB flux was admitted again and the rate measured. The result is presented in fig. 12b. The initial rate is higher than before but the decay is much faster. Post-reaction analysis showed a strongly reduced K-content

(I_K/I_{Fe}≈0.6) and strong coking (I_C/I_{Fe}=4.4). Control measurements revealed that the strong K-reduction had occurred during the "regeneration" in water and not during the second conversion measurement.

That water causes K-depletion is understandable. If KOH is formed at the surface, this may evaporate eventually because its vapor pressure at the reaction temperature is about 0.1 mbar. That the depletion is much slower in presence of EB means that the presence of carbon is necessary to avoid excessive K-depletion. A coke layer may directly protect the substrate from K-removal but in this case also the conversion activity would suffer. A result of K-promotion is just that the equilibrium amount of coke is lowered. A more likely possibility is the formation of carbonate. It was proposed that K_2CO_3 formation is part of a cyclic process by which coke is removed. Oxidic K reacts with water to form KOH which – competing with desorption – reacts with carbon to form K_2CO_3. The cycle is closed by thermal decomposition of carbonate into CO_2 which goes off and K-oxides which remain[43,44].

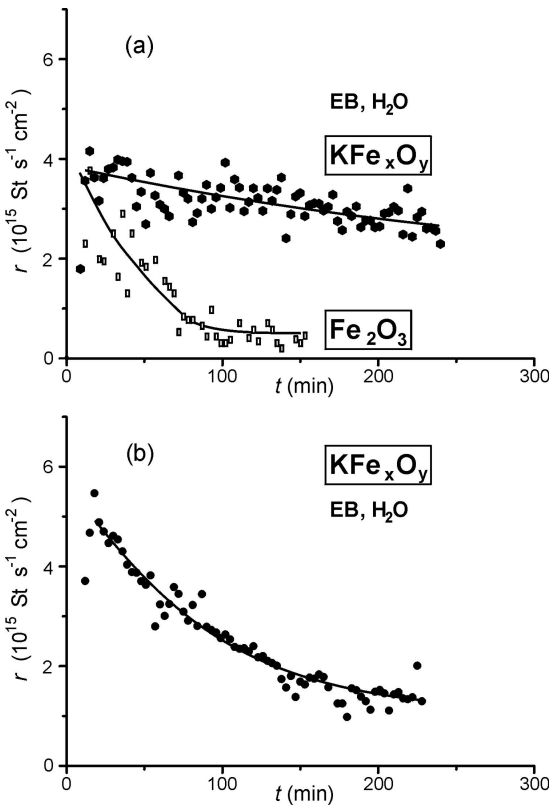

Figure 12: (a) St conversion over a K-promoted catalyst with intermediate K-content (upper curve) and unpromoted Fe_2O_3 (lower curve) under normal conditions (see table 1). (b) St conversion after "regeneration" of the K-promoted catalyst from (a) for 15 min with only H_2O and no EB in the feed, resulting in a low K-content.

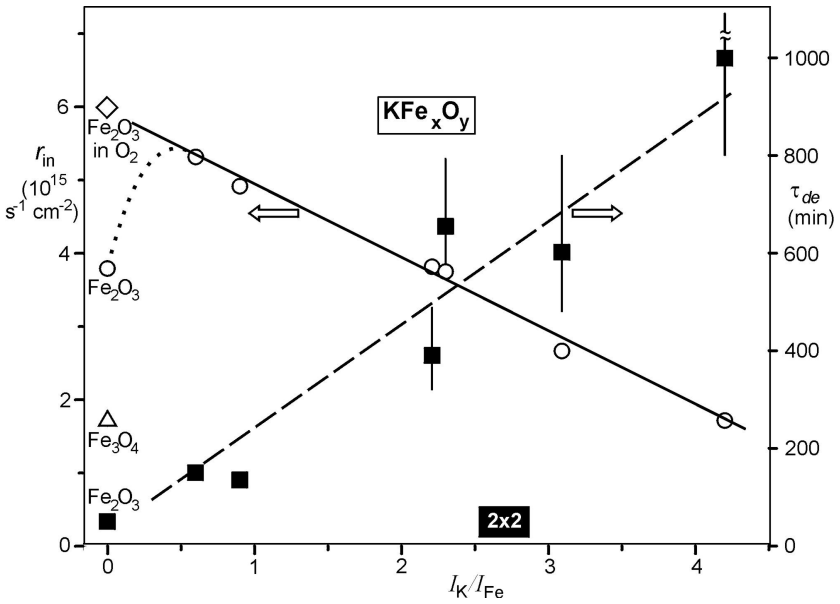

Figure 13: Initial St conversion rate r_{in} and time constant for deactivation t_{de} for samples with different initial K-content in terms of the Auger peak height ratio I_K/I_{Fe}. The composition where the ordered (2´ 2) structure is formed is indicated.

Fig. 13 summarizes the dependence of the initial conversion rates r_{in} and of the time constant of deactivation t_{de} (assuming an exponential decay of the rates) on the K-content in terms of I_K/I_{Fe} [36]. Also the initial rates for the unpromoted samples (Fe_2O_3, Fe_3O_4, Fe_2O_3 with O_2 added to the feed) are included. The initial rate decreases and the time constant for deactivation increases with growing K-content. Obviously, K prevents catalyst deactivation by reduction and coking but at the same time excess K reduces or blocks active surface sites. For I_K/I_{Fe}>2.7, the surface is increasingly covered by $KFeO_2$ [21,24]. The further decrease of the rate in this range proves that $KFeO_2$ is not the catalytically active phase. However, if it represents a K-reservoir, it may be responsible for slow deactivation. For practical applications, slow deactivation may be the decisive property.

For low K-content, the initial rate in fig. 13 tends towards the rate of Fe_2O_3 with O_2 in the feed while the rate of Fe_2O_3 without O_2 is lower (dotted curve). Most likely this is caused by partial deactivation of Fe_2O_3 before the first data point of the rate curve (fig. 10a) can be taken. It is plausible to assume that the topmost surface layer is partially reduced quite quickly so that the rate approaches that of Fe_3O_4 while addition of O_2 prevents this.

That potassium also prevents reduction of the catalyst was checked by using a catalyst with moderate K-content (I_K/I_{Fe}=1.2) for a conversion measurement with EB but without water in the feed, i.e. under the same conditions as for the unpromoted film in fig. 11 (lower curve). After 45 min, the surface composition was checked by AES. While the I_O/I_{Fe} ratio on the unpromoted film had decreased due to substrate reduction, it was essentially unchanged on the promoted catalyst.

3.5. Discussion

A striking result of the rate measurements is that the initial activities on unpromoted Fe_2O_3 and on promoted films are quite similar. The main role of potassium seems to prevent coking or to accelerate its removal and to prevent catalyst reduction. It is suggestive to assume that the active sites and mechanisms are the same and are related to stable Fe^{3+}. Because of not too

different apparent activation energies, this has already been proposed for polycrystalline and technical catalysts [45,46]. However, in this case the activity of the unpromoted catalyst was an order of magnitude lower than for the promoted catalyst. According to the model catalysis results reviewed here, this means that the unpromoted catalyst was most likely deactivated, i.e. reduced and coked. The model catalysis experiments showed that indeed the activity on the deactivated catalyst is about an order of magnitude lower but not zero. Most likely it is related to the catalytic activity of carbon.

The addition of oxygen does not so much influence the initial activity on Fe_2O_3 but rather the deactivation behavior. This suggests that the mechanism of the main reaction path is not influenced by the presence of oxygen. It is not oxidative in the sense that oxygen takes directly part in the catalytic reaction. It rather balances the effects of catalyst reduction by the hydrogen formed in the catalytic reaction and by coking, both being side reactions of the process. And it oxidizes the deposited carbon.

The active site requires Fe^{3+}. However, Fe_3O_4 is not equally active although it also contains Fe^{3+}. It could be that a pure Fe^{3+} environment is necessary as present in Fe_2O_3, $K_2Fe_{22}O_{34}$ and $KFeO_2$. But the study of the initial rates summarized in fig. 13 showed that $KFeO_2$ is obviously not more active than Fe_3O_4. An alternative and still more likely explanation was discussed by Kuhrs et al. [28] on the basis of the binding energies of EB and St on the different model catalysts (see fig. 6). Due to the existence of iron in the top layer of Fe_3O_4, both EB and St are bound so strongly that they block the surface under reaction conditions while the interaction with Fe_2O_3 and $K_xFe_{22}O_{34}$ is sufficient to bind the EB molecule long enough to the surface to enable dehydrogenation but neither EB nor St so strongly that they block the surface. On Fe_2O_3, St is bound more strongly than EB, but on $K_xFe_{22}O_{34}$ this difference disappears. Addition of K thus lifts product inhibition.

Based on the observations that both the right adsorption strength and – at least on unpromoted Fe_2O_3 – defects are necessary for high conversion, a model for the catalytic cycle has been proposed [28]. The adsorbate-substrate bond via the π-system of the benzene ring is responsible for holding the molecules long enough on the surface. Probably, they are mobile at the reaction temperature. If they meet a defect site exposing basic oxygen which attracts the H atoms, the ethyl group may be dehydrogenated. Simultaneously, two Fe^{3+} ions in the vicinity are formally reduced to Fe^{2+} which explains why Fe^{3+} is necessary and why iron with its variable valency is essential. The formed styrene desorbs. The hydrogen could desorb in form of H_2O by consuming a substrate O-atom which later would have to be replaced by dissociation of water or by reaction with O_2 from the feed. On the basis of the presented results, such a Mars-Van Krevelen mechanism cannot be ruled out completely although the high initial conversion without water in the feed suggest that a direct desorption in form of H_2 is also possible.

In fact, substrate oxygen is consumed but this is a side reaction and leads eventually to reduction of the substrate to Fe_3O_4. If only H_2O but no O_2 is added to the feed, this substrate reduction is irreversible.

So far, the structure of the anticipated K-carbonate protection layer on the promoted catalyst is unknown. It is feasible that the local structure of the active sites consists of O above three-valent Fe as in the case of unpromoted Fe_2O_3 while surface K carries a carbonate adsorbate group, possibly by inclusion of surface O.

In the literature, $KFeO_2$ was observed on the active promoted catalyst and was found to be essential for high and long-term activity. Therefore it was proposed to represent the catalytically avtive surface phase [47,48,48,49] while K-β-ferrite $K_2Fe_{22}O_{34}$ as bulk phase below was proposed to represent a K reservoir for the reestablishment of $KFeO_2$. Indeed, the model catalyst studies (section 2.3) [21,24]. showed that $KFeO_2$ forms when a layer of K

deposited on Fe_3O_4 is annealed at 700 K. Annealing to the reaction temperature 870 K results in a thin $KFeO_2$ layer on a possibly K-deficient K-β-ferrite. However, the dependence of the initial activity on K-content (fig. 13) showed that such a $KFeO_2$-containing sample (with high K-content) is much less active than samples with low K-content. Most likely, the roles of active phase and reservoir phase are inverted, i.e. K-β-ferrite is the active phase and $KFeO_2$ represents the K reservoir which intuitively seems quite plausible. The reservoir phase is necessary to reestablish stoichiometric K-β-ferrite under the conditions of continuous slow K-removal while the stoichiometry quickly drops when the reservoir phase is consumed. The existence of $KFeO_2$ would thus "buffer" the K-β-ferrite phase against K-depletion by reaction with H_2O.

When not enough K is deposited or when K is removed by steaming**,** the initial activity is high but deactivation is fast. We believe that this fast deactivation happens when the K content is too low to form a full Fe-O-K surface layer. Since surface and bulk composition are equilibrating quickly at the high reaction temperature, this surface layer can only be established when the bulk contains an amount of K which corresponds at least to substoichiometric $K_xFe_{22}O_{34}$ ($x \geq 0.67$).

After establishing steady-state conditions, the model catalysts and surely also real catalysts are always totally (unpromoted samples) or partially (K-promoted samples) covered by carbonaceous deposits. Also this coke is catalytically active as has been demonstrated here for the unpromoted catalyst. On the promoted catalysts, the contribution of coke to the catalytic conversion is not well established. K plays an important role in coke removal but at the same time it might act as polymerisation catalyst for the product St, possibly leading to graphitic deposits. Oxidative dehydrogenation studies of EB over carbon catalysts have shown that graphite, nanofilaments and nano-onions are highly active[41,42] while soot is not[50]. So far it is not known, what kind of carbon deposits are formed in absence and in presence of K on the catalysts and what their activity in presence of H_2O or O_2 is.

4. SUMMARY AND OUTLOOK

An in-depth study on a complex model catalysis system has been reviewed. The model reaction is the dehydrogenation of ethylbenzene to styrene in the presence of steam over unpromoted and K-promoted iron oxides. The study consists of a systematic and detailed analysis of the structure, composition and adsorption properties of 10-20 nm thick epitaxially grown model catalyst films of the composition Fe_xO_y and KFe_xO_y, followed by in-situ reactivity experiments at different pressures of the reactive gases: 3.5×10^{-6} mbar, 0.6 mbar and 36 mbar, always at the reaction temperature of 870 K and always with EB:H_2O ratios similar to real catalysis. The bridge over the pressure gap has thus several supports and is quite safe.

In order to be catalytically active, the surface of unpromoted Fe_2O_3 has to contain defects. At sufficiently high pressures, these defects are obviously created during reaction. Deactivation is accompanied by reduction to Fe_3O_4 and by coking. This agrees with powder catalyst studies but it had not been realized before that the initial activity was much higher and reached the level of promoted catalysts. By addition of low concentrations of oxygen, reduction and coking can be avoided and the high conversion level maintained. This may open a new reaction route using oxygen instead of promotion with K. It is an engineering problem to implement it and to make sure that no explosive $O_2 - H_2$ mixtures form.

Promoted catalysts deactivate more slowly because coke is more effectively removed and substrate reduction is avoided. This is in line with results on powder catalysts. Apart from one special composition ($K_xFe_{22}O_{34}$, $x \approx 0.7$), promoted model catalysts cannot be prepared with a

long-range ordered surface. With the available in-situ surface science methods, disorder could therefore not be identified as essential for catalytic activity. However, the similarity of the initial activities of promoted and unpromoted model catalysts suggests the same mechanism. This has to be proven in future.

Since the model catalysts are free of pores, the observed conversions could easily be referred to the active geometric surface. Conversion rates are in the range of 1 to 10×10^{15} styrene molecules per cm^2 and s. The corresponding turnover frequencies (TOF) are of the order of 10 per site and s or even higher if the concentration of active defects is low. The catalytic activity is thus quite high. The limitation in technical catalysis is rather the accessibility of the catalyst surface as well as matter and energy transport.

For a number of mechanistic details, it was important that the model catalysts consisted of a limited amount of material in the form of thin films. It could easily be shown that the oxygen liberated during reduction of Fe_2O_3 is not responsible for the main dehydrogenation reaction path of ethylbenzene in a stoichiometric reaction but that the main reaction is catalytic.

Also the processes of K depletion could only be observed and assigned so clearly because the thin film contained a limited amount of K. At reaction temperature, K diffusion over distances of the film thickness is fast. Its distribution is always near to equilibrium and leads to K accumulation in the topmost layer. As long as the bulk concentration is high enough to maintain a stoichiometric Fe-O-K surface composition, deactivation is slow. Lower K concentrations even increase the initial activity but this is quickly compensated by a faster deactivation. Not unexpected, the presence of pure water causes fast K-depletion by formation of KOH which evaporates. A surprising observation was that this depletion is much slower when ethylbenzene is admitted. Obviously, a surface compound is formed in the presence of EB and its reaction products (St, CO_2, coke…) which attenuates K removal. A candidate is K_2CO_3 which is also likely to be involved in coke removal.

The existence of Fe^{3+} is necessary but obviously not sufficient for high catalytic activity since also the much less active compounds Fe_3O_4 and $KFeO_2$ contain Fe^{3+}. It is likely that the adsorption strength for EB and St is decisive. On Fe_2O_3 and $K_xFe_{22}O_{34}$ it is similar and low while it is much higher on Fe_3O_4 because of the existence of Fe atoms in the top atomic layer. Site blocking is therefore the likely reason for its low activity.

Still, the proposed defect mechanism is hypothetical and the nature of the defects is unknown. But that defects are essential is a result of the combination of surface analysis by surface science methods with in-situ reactivity studies under conditions relevant to real catalysis.

The steady-state activity of the unpromoted catalyst (termed “deactivated” in this study) is due to carbonaceous deposits. Their activity is low but definitely non-zero. The activity of the always present carbonaceous deposits on promoted catalysts needs further investigations.

The presented study demonstrates that the model catalysis approach yields essential contributions for a deeper understanding of catalysis. But it demonstrates also that this is a long way to go. Improvements of the technological processes on the basis of model catalytic results are feasible. Many questions remain still open. Next steps will be the inclusion of transport phenomena by the use of porous samples in the model catalysis setup and the modeling of the properties and behaviour of a real system using insights and data from the model study.

ACKNOWLEDGEMENT

Discussion and support by Robert Schlögl is gratefully acknowledged. The work was supported by the Deutsche Forschungsgemeinschaft, grant no. RA 376/2-2.

REFERENCES

1. Ertl G., and Küppers, J. 1985, Low Energy Electrons and Surface Chemistry, 2nd ed., VCH, Weinheim.
2. Somorjai, G. A. 1994, Surface Chemistry and Catalysis, John Wiley& Sons, Inc., New York.
3. Ertl, G., Knözinger J., and Weitkamp, J. (Eds.) 1997, Handbook of Heterogeneous Catalysis, Wiley-VCH, Weinheim.
4. Blakely, D. W., Kozak, E. I., Sexton, B. A., and Somorjai, G. A. 1976, Journal of Vacuum Science & Technology 13**,** 1091.
5. Reichl, W., Rosina, G., Rupprechter, G., Zimmermann, C., and Hayek, K. 2000, Review of Scientific Instruments, 71**,** 1495.
6. Knop-Gericke, A., Hävecker, M., Schedel-Niedrig, T., and Schlögl, R. 2001, Topics in Catalysis, 15**,** 27.
7. Bukhtiyarov, V. I., Hävecker, M., Kaichev, V. V., Knop-Gericke, A., Mayer, R. W., and Schlögl R. 2003, Physical Review B, 67, 235422-1.
8. Haw, J. 2002, In-Situ Spectroscopy in Heterogeneous Catalysis, Wiley-VCH, Weinheim.
9. Weckhuysen, B. M. 2004, In-situ Spectroscopy of Catalysts, American Scientific Publishers.
10. Freund, H.-J., Ernst, N., Bäumer, M., Rupprechter, G., Libuda, J., Kuhlenbeck, H., Risse, T., Drachsel, W., Al-Shamery, K., and Hamann, H. 2002, Surface chemistry and catalysis, Carley, A. F., Davis, P. R., Hutchings, G. J., and Spencer, M. S. (Eds.), Kluwer Academic/Plenum Publishers, New York.
11. Miura, H., Kawai, H., and Taguchi, T. 1994, Studies on Surface Science and Catalysis, 90, 461.
12. Joseph, Y., Wühn, M., Niklewski, A., Ranke, W., Weiss, W., Wöll, C., and Schlögl, R. 2000, Physical Chemistry Chemical Physics, 2, 5314.
13. Weiss, W., and Ranke, W. 2002, Progr Surf Sci, 70, 1.
14. Ritter, M.; Over, H.; and Weiss, W. 1997, Surface Science, 371, 245.
15. Ketteler, G., and Ranke, W. 2003, Materials Research Society Symposium Proceedings, 775, P6.1.1.
16. Ketteler, G., and Ranke, W. 2003, Journal of Physical Chemistry B, 107, 4320.
17. Koveshnikov, A. N., Madjoe, R. H., Karunamuni, J., Stockbauer, R. L., and Kurtz, R. L. 2000, Journal of Applied Physics, 87, 5929.
18. Ketteler, G., Weiss, W., Ranke, W., and R. Schlögl, W. 2001, Physical Chemistry Chemical Physics, 3, 1114.
19. Fadley, C. S., Van Hove, M. A., Hussain, Z., and Kaduwela, A. P. 1995, Journal of Electron Spectroscopy and Related Phenomena, 75, 273.
20. Shaikhutdinov, Sh. K., Meyer, R., Lahav, D., Bäumer, M., Klüner, T., and Freund, H.-J. 2003, Physical Review Letters, 91, 076102-1.
21. Joseph, Y., Ketteler, G., Kuhrs, C., Ranke, W., Weiss, W., and Schlögl, R. 2001, Physical Chemistry Chemical Physics, 3, 4141.
22. Ritter M., and Weiss, W. 1999, Surface Science, 432, 81.
23. Ketteler, G., Weiss, W., and Ranke, W. 2001, Surface Review and Letters, 8, 661.
24. Ketteler, G., Ranke, W., and Schlögl, R. 2002, Journal of Catalysis, 212, 104.
25. Ranke, W. and Weiss, W. 1998, Surface Science, 414, 236.
26. Ranke, W. and Joseph, Y. 2002, Physical Chemistry Chemical Physics, 4, 2483.
27. Joseph, Y., Ranke, W., and Weiss, W. 2000, Journal of Physical Chemistry B, 104, 3224.

28. Kuhrs, C., Arita, Y., Weiss, W., Ranke, W., and Schlögl, R. 2001, Topics in Catalysis, 14, 111.
29. Shaikhutdinov, S. K., Joseph, Y., Kuhrs, C., Ranke, W. and Weiss, W. 1999, Faraday Discussions, 114, 363.
30. Masel, R. I. 1996, Principles of Adsorption and Reaction on Solid Surfaces, John Wiley& Sons, New York.
31. Zscherpel, D. 1998, PhD Thesis, Freie Universität Berlin, FB Chemie, Berlin.
32. Ranke, W. and Weiss, W. 2000, Surface Science, 465, 317.
33. Weiss, W., Zscherpel, D., and Schlögl, R., Catalysis Letters, 52, 215.
34. Shekhah, O., Ranke, W., Schüle, A., Kolios, G., and Schlögl, R. 2003, Angewandte Chemie, Int. Ed., 42, 5760.
35. Shekhah, O., Ranke, W., Schüle, A., Kolios, G., and Schlögl, R. 2003, Angewandte Chemie, 115, 5938.
36. O. Shekhah, W. Ranke, and R. Schlögl. 2004, Journal of Catalysis, submitted.
37. Muan, A., 1958, American Journal of Science, 256, 171.
38. Ketteler, G. 2003, private communication.
39. Kochloefl, K. 1997, Handbook of Heterogeneous Catalysis, Ertl, G., Knözinger, J., and Weitkamp, J. (Eds.) 1997, VCH, Weinheim, Vol. 5, p. 2151.
40. Meima, G. R., and Menon, P. G. 2001, Applied Catalysis A, 212, 239.
41. Mestl, G., Maksimova, N. I., Keller, N., Roddatis, V. V., and Schlögl, R. 2001, Angewandte Chemie, Int. Ed,. 40, 2066.
42. Keller, N., Maksimova, N. I., Roddatis, V. V., Schur, M., Mestl, G., Butenko, Y. V., Kuznetsov, V. L., and Schlögl, R. 2002, Angewandte Chemie, Int. Ed., 41, 1885.
43. Lee, E. H. 1973, Catalysis Review, 8, 285.
44. Coulter, K., Goodman, D. W., and Moore, R. G. 1995, Catalysis Letters, 31; 1.
45. Hirano, T. 1986, Applied Catalysis, 26, 65.
46. Addiego, W. P., Estrada, C. A., Goodman, D. W., Rosynek, M. P., and Windham, R. G. 1994, Journal of Catalysis, 146, 407.
47. Hirano, T. 1986, Applied Catalysis, 28, 119.
48. Muhler, M., Schütze, J., Wesemann, M., Rayment, T., Dent, A., Schlögl, R., and Ertl, G. 1990, Journal of Catalysis, 126, 339.
49. Muhler, M., Schlögl, R., and Ertl, G. 1992, Journal of Catalysis, 138, 413.
50. Maksimova, N. I., Roddatis, V. V., Mestl, G., Ledoux, M., and Schlögl, R. 2000, Eurasian Chem. Tech. Journal, 2, 231.